


Handbook
for
Generic Photonic IC Design

Editors: Meint Smit and Xaveer Leijtens

4-4-2026

 *Handbook for generic photonic IC design*, by the *Photonic Integration group*, Technische Universiteit Eindhoven, is licensed under a Creative Commons “Attribution-NonCommercial-NoDerivatives 4.0 International” license.

We traced the ownership of all figures used as far as we could. However, if you are a copyright owner and believe we used your work without permission, please contact us at coordinator@jeppix.eu.

Chapter 17

Modulators (draft)

WEIMING YAO AND MARIJA TRAJKOVIC

This chapter introduces the most relevant concepts for electro-optic modulator design on generic InP platforms. Electro-refraction and electro-absorption in ridge type InP waveguides are discussed and conventional EOPMs and EAMs are presented with emphasis on RF design methodologies.

17.1 Introduction

The purpose of the modulator component within an optical transmitter is the conversion of information from the electrical domain into the optical domain. It is one of the main components in any optical transmission link and has significant influence on its performance. Advancements in modulator design and development are therefore crucial for achieving high-capacity optical transmitters. We will present the working principle of the electro-optic phase modulator and the electro-absorption modulator and discuss design considerations for the generic InP PIC platform. Electro-optic effects in an InP ridge waveguide are first introduced and the quantum-confined Stark effect (QCSE) is briefly discussed in multiple quantum-wells. This chapter then goes into more detailed design guidelines for both the electro-optic phase modulator (EOPM) and the electro-absorption modulator (EAM). Accurate microwave modeling is introduced for both types as an enabling methodology to better understand the limitations on modulation speed and how to further enhance bandwidth.

Optical modulators can be based on different working principles where the electrical information is mapped onto properties of the optical signal. The optical carrier field has various properties that can be changed to encode information, for example intensity, phase or polarization [236]. Historically, the first optical communication systems worked with modulation of the optical signal intensity. Intensity modulation can be achieved either by directly changing the current to the laser source or by using an external modulator. In the former case, frequency chirping of the output optical signal is inevitable, which limits the transmission distance and capacity due to fiber chromatic dispersion [237]. The reason for this lies in the inherent coupling of the real and imaginary part of the index of refraction in semiconductor materials [238]. Whenever the absorption is changed by current modulation in the laser, the optical phase undergoes change as well, resulting in frequency broadening of the optical output. Furthermore

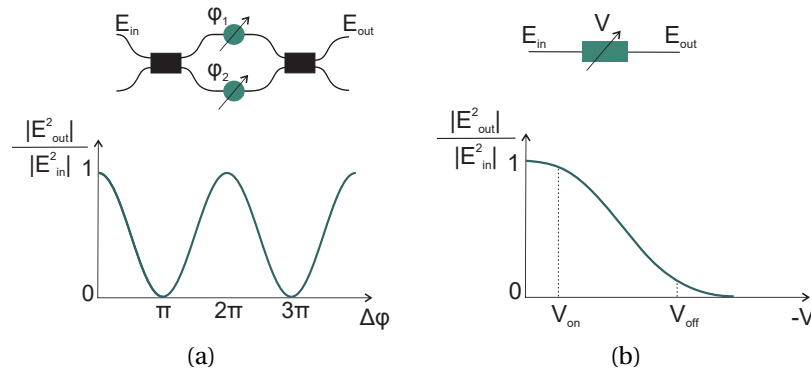


Figure 17.1: Structure and modulation of the optical intensity in case of (a) Mach-Zehnder and (b) electro-absorption modulators.

carrier dynamics in semiconductor lasers tend to have a limiting effect on modulation speed and additional care is needed for designing for high-speed operation. Therefore, external modulators have been widely used for high-capacity transmission systems, where the modulator design can be decoupled from the laser design and separately optimized.

Many types of external modulators exist, each with their respective advantages and drawbacks. A good overview can be found in [239]. The two most commonly used modulator types are the Mach-Zehnder modulator (MZM) and the electro-absorption modulator (EAM). The former is employed in most of the long-haul optical links as a high-performance, versatile modulator for advanced modulation formats, whereas the latter is used in short-reach applications such as in access and metropolitan networks due to their simple and cost-effective design. With the increasing bandwidth demands of data center networks recently, MZMs are more frequently used also for short-distance links with intensity modulation direct detection (IM/DD) in combination with multi-level modulation formats such as PAM-4 or PAM-8 [240]. Micro-ring modulators are a third common type that rely on resonance enhancement and not further discussed here as they are narrow-band and more suited for high index-contrast waveguide platforms. Fig. 17.1 shows the working principle of both modulators. In a MZM the optical signal is split into two and propagates through two waveguides, where in each the optical phase can be changed depending on an applied voltage signal. At the end both waveguides are combined and the two optical signals superimpose at the output. Depending on the phase difference $\Delta\phi = \phi_2 - \phi_1$ between both arms of the MZM, the output signal is the result of either constructive or destructive interference and the intensity-phase relation is described by a cosine square function. In case of the EAM, the optical absorption is a function of applied voltage and the transmission through the device can be controlled in this way. The intensity-voltage relation shows a gradual and smooth decrease of transmission with increasing voltage values.

In terms of chirp performance, the MZM is preferred over the EAM, as the chirp of the output signal can be set in an exact way by controlling the propagation constants in each arm of the modulator, i.e. zero chirp output can be achieved when the propagation constants are equal in magnitude but opposite in sign [241]. This property of MZMs makes them ideal for long-haul applications where zero chirp or negative pre-chirping can be achieved [242]. In contrast, EAMs suffer from the same inherent link between intensity and phase modulation as in directly modulated lasers. Although it is possible to control the chirp parameter of the output pulses in case of EAMs, the

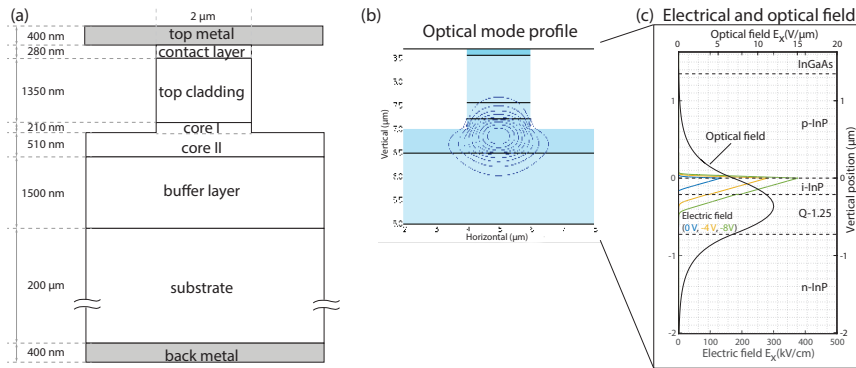


Figure 17.2: <missing caption>

method is not straight forward and restricts the bias voltage to specific values [243]. From a high-frequency point of view, both the EAM and the MZM are electrically decoupled from the laser source, so it is possible to optimize their microwave design separately from the laser and achieve high modulation speeds.

17.2 Ridge Waveguide Modulators

In this section we look at the modeling and working principle of a waveguide modulator building block on the generic integration platform (historically referred as the COBRA generic platform [1]). We first present a standard waveguide modulator structure that can be used for both an electro-optic phase modulator and an electro-absorption modulator and detail the static and dynamic analysis methodologies. Afterwards, limitations on modulator speed and efficiency are discussed for electro-optic and electro-absorption modulators.

The waveguide modulator consist of a standard optical waveguide that is electrically in contact with a microwave transmission line. The design of the transmission line and the underlying optical waveguide structure directly influences the modulator static and dynamic performance.

Fig. 17.2a shows the structure of the shallow ridge waveguide used in the COBRA platform. Light is guided in the core layer through total internal reflection, which is situated between a top cladding and a bottom buffer layer, both with lower refractive indices. This waveguide structure allows for the propagation of the fundamental and first order mode, both TE and TM polarized, due to the wide ridge width of $2\ \mu\text{m}$. A standard deeply etched waveguide with a ridge width of $1.5\ \mu\text{m}$ that only guides the fundamental mode can also be used to form a phase shifter. The latter has better microwave characteristics due to the lower junction capacitance. For the explanation of the modeling methodology that applies to both waveguides, we will use the former, the shallow waveguide. The waveguide width will have an effect on the electro-optic bandwidth of the modulator and will be discussed later in this chapter.

Fig. 17.2b depicts the optical field distribution of the fundamental TE mode for the shallow waveguide. The results are obtained from simulations performed using FIMMWAVE [181]. Material parameter for each layer can be taken from [244]. The refractive indices for the different layers and compositions can be obtained using the modified single oscillator model [245].

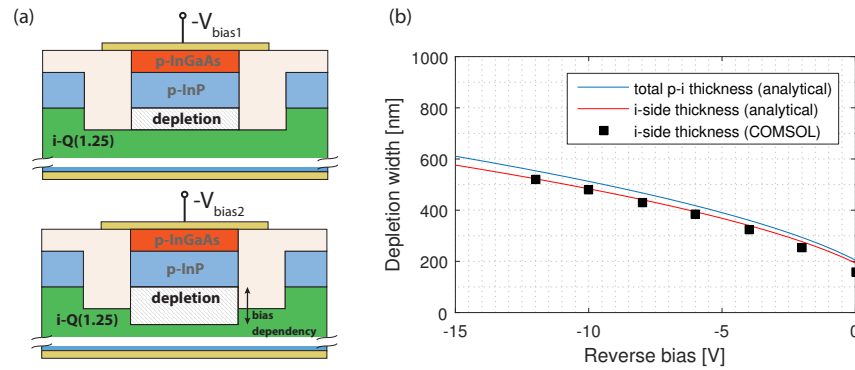


Figure 17.3: (a) Schematic illustration of bias dependent depletion zone. (b) Calculated and simulated depletion thicknesses for varying bias voltages. The analytical result agrees well with the COMSOL simulations. The modulation of the thickness can be estimated analytically according to the Shockley model [246].

The exact layer design in the COBRA platform has been previously optimized for low optical loss and high electro-optic efficiency. The quaternary core layer Q-1.25 (bandgap 1.25 μm) is separated from the p-InP cladding through an intrinsic InP buffer layer (core I), whose purpose is to separate the optical mode field from the lossy p-cladding. This can be seen in Fig. 17.2c where the optical mode is centered around the Q-1.25 layer. Both the buffer layer and the core layer have been previously tuned in terms of doping concentration to allow for a good trade-off between optical loss and electric field strength. As can be also seen from Fig. 17.2c, the electric field at varying reverse bias voltages has different penetration depths into the core area. At 0 V the built-in potential difference between the p-doped InP and the non-intentionally doped InP generates an electric field that sweeps out the carriers, creating a depletion region. With increasing reverse bias, the depletion area grows into the direction of the core layer until it reaches a thickness of several hundred nanometers. The depletion into the p-InP remains under 100 nm through this process.

From an electrical point of view this waveguide is a typical p-i-n hetero-junction. A depletion area without any carriers is formed in the structure. The change in thickness according to an externally applied voltage as can be seen in Fig. 17.3.

This build-up of electric field together with the depletion of carriers causes a change in the effective refractive index and absorption seen by the optical mode. This effect strongly depends on the overlap of the two mechanisms, i.e. depletion of carriers and electric field, with the optical intensity distribution. Therefore, the core layer doping concentration influences the electro-optic interaction. A high doping leads to a reduced depletion zone, resulting in smaller carrier induced effects. The electric field is stronger, but the total overlap with the optical mode is also reduced. Furthermore, optical absorption due to dopants increases. A doping concentration which is too low widens the depletion zone. Although the overlap of the electric and optical field increases, the electric field strength is reduced and the strength of carrier based effects is also reduced. A good compromise of $6 \cdot 10^{16} \text{cm}^{-3}$ has been identified from previous studies [114].

Static modelling of the electro-optic interaction in the phase-shifter can be performed in two parts. At first, the electric field distribution and depletion thickness in the core layers need to be obtained. In a second step, the electro-optic interaction can be estimated and the effective index change and absorption change that is seen by the optical

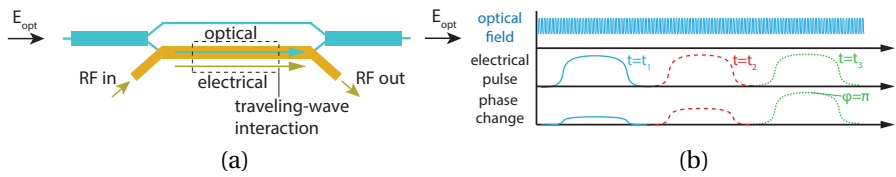


Figure 17.4: (a) Schematic showing a traveling-wave electrode on a MZM. (b) interaction of a propagating microwave and optical CW-signal at different times and locations along the propagation direction.

signal is calculated. From that, the phase change in case of electro-refractive or transmission change in case of electro-absorption modulator for a given length and voltage can be calculated.

17.3 Electro-optic phase modulator (EOPM)

17.3.1 Traveling-Wave operation

To construct an EOPM, the ridge waveguide modulator concept is used in combination with a core layer (bulk or MQW) that is optimized for electro-refraction as discussed before. This section presents the guidelines to reach high-speed operation for EOPMs.

Most of the recent high-bandwidth phase modulators utilize a traveling-wave electrode instead of a lumped element electrode to carry the electrical data signal. A lumped electrode exhibits a certain capacitance and together with a finite series resistance, its RC charge and recharge time limits the usable modulation speed. This capacitance can be circumvented by using a traveling-wave approach, where the microwave signal propagates from the start of the electrode to its end. The electrode behaves as a transmission line and the signal only sees the transmission line capacitance per unit length and not the capacitance formed by the total electrode so that RC roll-off is effectively overcome [247]. Further increase in modulation speed can be achieved if both the electrical signal and the optical signal are matching their propagation speed, so that the interaction takes place at the same relative location throughout the length of the modulator [248].

Fig. 17.4a depicts the structure of a traveling-wave electrode used in a Mach-Zehnder configuration which is discussed in a later chapter. The traveling-wave electrode is defined on either one or both arms of the Mach-Zehnder interferometer. The RF data signal is fed from the left and co-propagates with the underlying optical signal. During the propagation along the electrode, the electro-optic interaction takes place. In the ideal case, the optical and electrical group velocities are matched and their interaction accumulates along the whole electrode length as shown in Fig. 17.4b. As a result the local phase change stays at the same place of the optical envelope and travels along the electrode. The traveling-wave electrode needs to be properly terminated at the right end to reduce electrical reflections which could perturb the driving signal.

A simple way to demonstrate the advantage of the traveling-wave approach over the lumped electrode in terms of modulation speed is to estimate the 3dB bandwidth in both cases. The RC limited bandwidth can be calculated as

$$f_{\text{lumped}} = \frac{1}{2\pi RC}, \quad (17.1)$$

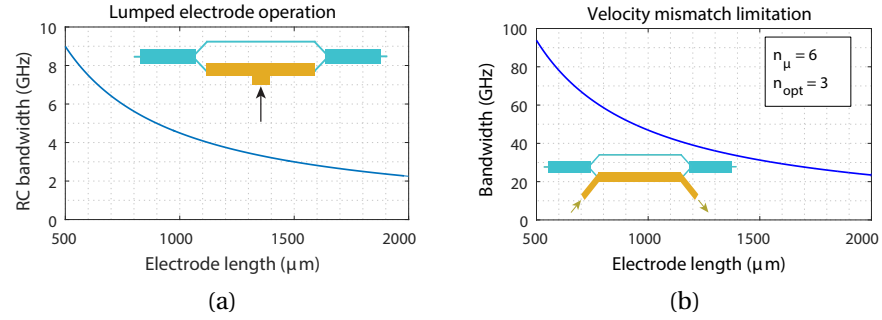


Figure 17.5: Calculated modulation bandwidth in case of (a) a lumped element electrode with 2 μm ridge waveguide width and (b) a traveling-wave electrode with velocity mismatch factor of 2 for COBRA phase-shifting sections.

with R the access resistance and C the lumped electrode capacitance. Fig. 17.5a depicts the achievable bandwidth for a waveguide width of 2 μm, depending on the electrode length L , assuming $R = 50\Omega$ and a parallel plate capacitor approximation for the modulator capacitance.

In case of a traveling-wave electrode, it can be shown that the modulation bandwidth is limited by the velocity mismatch between the optical and electrical signal, when we assume ideal conditions¹ [249]:

$$f_{TW} = \frac{1.4c}{\pi|n_{opt} - n_{\mu}|L}, \quad (17.2)$$

with c the vacuum light velocity, n_{opt} and n_{μ} the effective optical and microwave index and L the electrode length. Fig. 17.5b shows that even in case of a velocity mismatch of factor 2 the traveling-wave approach exhibits much higher modulation bandwidth. The walk-off becomes only a limitation above 40 GHz for typical MZM lengths of 1.3 mm in the COBRA integration platform. Below that frequency, impedance mismatch and microwave attenuation are the limiting factors for traveling-wave modulators [250, 251].

A typical way to define the traveling-wave electrode is to employ common microwave transmission line geometries such as coplanar waveguide (CPW) or coplanar stripline (CPS) electrodes. The CPW electrode is very simple to implement in the COBRA integration platform and consists of a signal electrode between two ground electrodes. Fig. 17.6 shows the top and cross section view of such a CPW electrode placed on top of the ridge waveguide modulator structure. The signal electrode is in contact with the p-side of the waveguide whereas the ground electrodes make contact laterally to the n-doped InP that is connected to the n-side of the waveguide. This allows for adjusting the reverse bias needed for the operation of the EOPM. Due to the built-up of a depletion area in the waveguide, most of the high-speed signal field is concentrated in that area, contributing to the modulation of the refractive index.

17.3.2 Electro-optical modelling

In order to achieve broadband, high-speed operation, the CPW transmission line needs to be optimized with respect to impedance matching, velocity matching, minimum microwave attenuation and maximum electric field drop across the optical waveguide. A very useful methodology is to model the transmission line with distributed

¹Zero microwave loss and no impedance mismatch

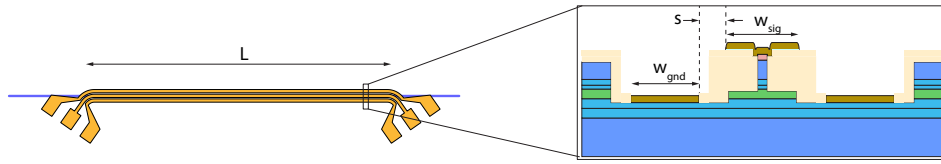


Figure 17.6: <missing caption>

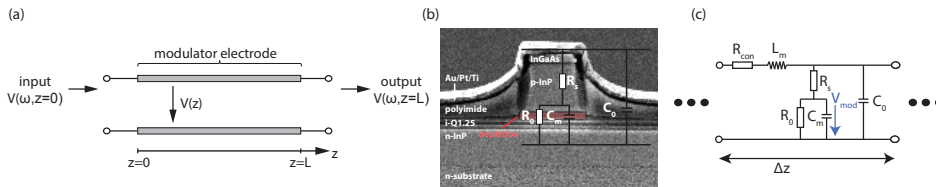


Figure 17.7: <missing caption>

equivalent circuits. Such circuit elements are defined per unit length and can accurately model the signal propagation along transmission lines and is standard practice for microwave engineering [252]. Two approaches can lead to the determination of circuit elements. Either they are calculated from geometrical considerations using e.g. inspection data from cross sections or transmission line test structures can be characterized and circuit elements extracted from the measured scattering parameters. Fig. 17.7 shows how a distributed equivalent circuit can be built from geometrical analysis of the EOPM cross section using scanning electron microscope images.

Once the equivalent circuit model is constructed, the modulating signal along the EOPM can be readily computed to model the electro-optic interaction and estimate the small-signal or large-signal modulation response. Detailed methodologies for this are given in [253].

17.3.3 Bandwidth-Efficiency Trade-Off

From Fig. 17.5 we observe that the bandwidth of the modulator depends on its electrode length both in case of lumped and traveling-wave operation. In fact the lumped operation with sufficient long L can be seen as a traveling-wave configuration where the input feed is positioned at the transmission line center, so that two waves propagate towards the start and end of the lumped electrode. Its standing-wave pattern imposes the lumped element RC limitation [254]. Longer electrodes have more accumulated electro-optic interaction and therefore require less drive-voltage. However, due to a larger propagation distance of the electric drive signal, microwave losses will attenuate it, resulting in a drop in electro-optic bandwidth. This trade-off between drive voltage and modulation bandwidth is characteristic for electro-optic modulators and depends among others on the specific technology used. The COBRA platform with a bulk Q-1.25 waveguide exhibits a relatively weak electro-optic effect when compared to multi quantum-well core material. Fig. 17.8 shows the voltage needed to achieve π phase change, the so-called half-wave voltage V_{π} , for COBRA EOPMs based on bulk core material. A smaller half-wave voltage is desired to minimize voltage swing from the driver and system power consumption. This can be acquired by making the EOPM longer. However, that is in trade-off with accumulated microwave losses that reduce the EOPM bandwidth. Reduction in microwave loss or increase in electro-optic efficiency can both directly influence this trade-off.

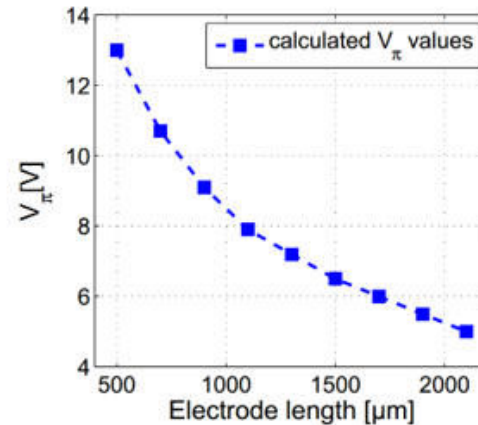


Figure 17.8: <missing caption>

The choice of modulator core material is the result of many considerations and compromises that weight the functionality of a palette of active and passive building blocks against the fabrication challenges and risks associated with a more complex process flow for multi-project wafer runs. Recent research projects have introduced MQW core material to the COBRA platform for the EOPM building block. Together with an optimized transmission line geometry in form of CPS electrodes, this has significantly improved the high-speed operation. Such CPS modulators have been shown to operate beyond 100 GHz at 160 Gbaud modulation [255].

17.4 Electro-absorption modulator (EAM)

Electro-absorption modulators can be made much shorter than EOPMs due to its absorptive nature. This is especially beneficial for short-reach optical communications, where small sized low-cost devices are needed. For EAMs, drive voltage reduction, bandwidth increase and optimizing extinction ratio are all important aspects. Various methods have been studied for that.

In order to reduce the EAM drive voltage some of the work explored a dual-depletion region and an undercut etch, reducing the DC drive to -1 V [256, 257]. Comparing the swing voltage of a MZM and EAM, the resulting value is 2 V for both modulator types. Other work, that focused on optimizing the swing voltage, shows values as low as ~0.8 V [258, 259].

For high speed operation two approaches have been investigated – lumped and travelling wave configuration [260]. An EML with a travelling wave (TW) modulator configuration showed 100 GHz bandwidth [261, 262]. For high density circuits lumped EAM allows more components to be integrated on a single chip. To efficiently increase the bit rate per channel without requiring proportional increase in the bandwidth, the use of higher order modulation formats is essential [263]. For intensity modulation/direct detection (IM/DD) systems Pulse Amplitude Modulation (PAM-N, where N represents the number of levels) is currently being standardized in short-reach applications.

Finally, an optimized electro-absorption modulator requires a separate layer stack for a minimal insertion loss, a high number of quantum wells (QWs) for high extinction ratio [264], quantum wells based on aluminum quaternaries (InGaAlAs rather than In-

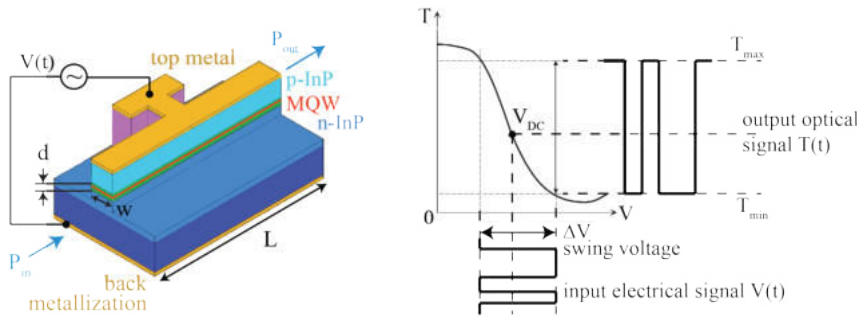


Figure 17.9: 3D illustrated view of an electro-absorption modulator and its transfer (transmission) curve $T(V)$.

GaAsP) for a large temperature operation range [265], and a thick dielectric or semi-insulating substrate for an improved radio-frequency (RF) performance.

17.4.1 The EAM operation principle

Here we will consider a p-i-n diode structure, consisting of a multi-quantum well (MQW) structure, shown in Fig. 17.9. When an electric field is applied perpendicularly to the p-i-n structure, the absorption increases and the transmission (T) decreases, explained by quantum-confined Stark effect (QCSE) [266].

An important parameter for EAM operation is its DC bias voltage V_{DC} . The lower the value, the lower the total power consumption. For dynamic measurements it is desirable to be positioned in the centre of transmission response linear region (inflection point). In this case the transmission curve is linear and irrelevant of the modulation format at the input $V(t)$, its transfer signal will be linear at the output ($T(t)$). The required swing voltage ΔV should also be small to reduce the overall power consumption. In principle, steeper transfer curve needs lower swing.

Main parameters influencing the optical signal propagation are: intrinsic layer (i-InP) thickness d , waveguide width w , optical confinement factor in MQW Γ , and structure length L . These parameters will determine the behavior of the EAM and the shape of the transfer curve.

17.4.2 Optical design considerations

The design of an electro-absorption modulator involves a number of optical and electrical properties. Optical features include static extinction ratio, determining the modulator ability to suppress the input optical power, and the on-state insertion loss, determining the loss inside the modulator itself. The electrical characteristics include electro-optical bandwidth, determining the operating speed, drive voltage, and the electrical reflection parameter, affecting the electrical signal propagation. For successful implementation of EAMs in system applications a list of requirements include low insertion loss, low drive voltage, high bandwidth, low temperature sensitivity and low cost.

17.4.2.1 Static extinction ratio

The total insertion loss is defined as the ratio of the output over the input light intensity, and gives information about the total losses in the system as a function of the applied DC bias voltage. The ratio of the output power at different bias points and at $V = 0$ V gives the static extinction ratio (ER). The static ER is related to the absorption coefficient change $\Delta\alpha$ with the applied voltage, and confinement factor Γ . For a modulator of length L the extinction ratio can be written as:

$$\text{ER} = \frac{P_{\text{out}}(V = 0)}{P_{\text{out}}(V)} = \frac{e^{-\Gamma\alpha(0)L}}{e^{-\Gamma\alpha(V)L}} \quad (17.3)$$

$$\text{ER}_{\text{dB}} = 10 \log_{10} e^{-\Gamma\Delta\alpha L} = 4.343 \Gamma \Delta\alpha L \quad (17.4)$$

The absorption coefficient α is dependent on material properties (and the voltage induced electro-absorption from QCSE), whereas the confinement factor is a power fraction representing the overlap of the optical mode (described by $U(x, y)$) with the active layer, given by [203]:

$$\Gamma = \frac{\int_{-w/2}^{w/2} \int_{-d/2}^{d/2} |U(x, y)|^2 dx dy}{\int_{-\infty}^{\infty} \int_{-\infty}^{\infty} |U(x, y)|^2 dx dy} \quad (17.5)$$

The confinement factor for the active region of an EAM can be increased by increasing thickness of the active layer, i. e. increasing the quantum well number. However, increased confinement of the optical mode increases the effective index of the mode and shrinks its effective size. This can lead to a mode mismatch with the rest of structures having a different layer composition.

17.4.2.2 On-state insertion loss

The total insertion loss in the electro-absorption modulator is made out of three major components: absorption and scattering of the guided mode, and coupling loss due to spot-size mismatch between the waveguide and the edge-coupled fibre. The on-state insertion loss is the absorption loss in the active region when no external electrical field is present ($V = 0$).

$$IL_{\text{ON}} = \frac{P_{\text{in}} - P_{\text{out}}(V = 0)}{P_{\text{in}}} = 1 - e^{-\Gamma\alpha(0)L} \quad (17.6)$$

From the structure optimization standpoint view, a trade-off exists between the extinction ratio and the on-state insertion loss (seen from Eq. 17.4 and 17.6). Large detuning implies low IL_{ON} , but also poorer extinction ratio (from Fig. 3.23).

17.4.2.3 Temperature dependence

When the temperature of a semiconductor is increased, its crystal lattice expands and the absorption peak shifts to lower energies. Furthermore, the transmission curve is modified and has the effect as the detuning increase. Temperature variation effects are typically avoided with a use of thermo-electric cooler (TEC) [267]. However, this significantly increases power consumption and packaging cost. An EAM which can operate in a wide temperature range is advantageous as it will decrease the overall power consumption.

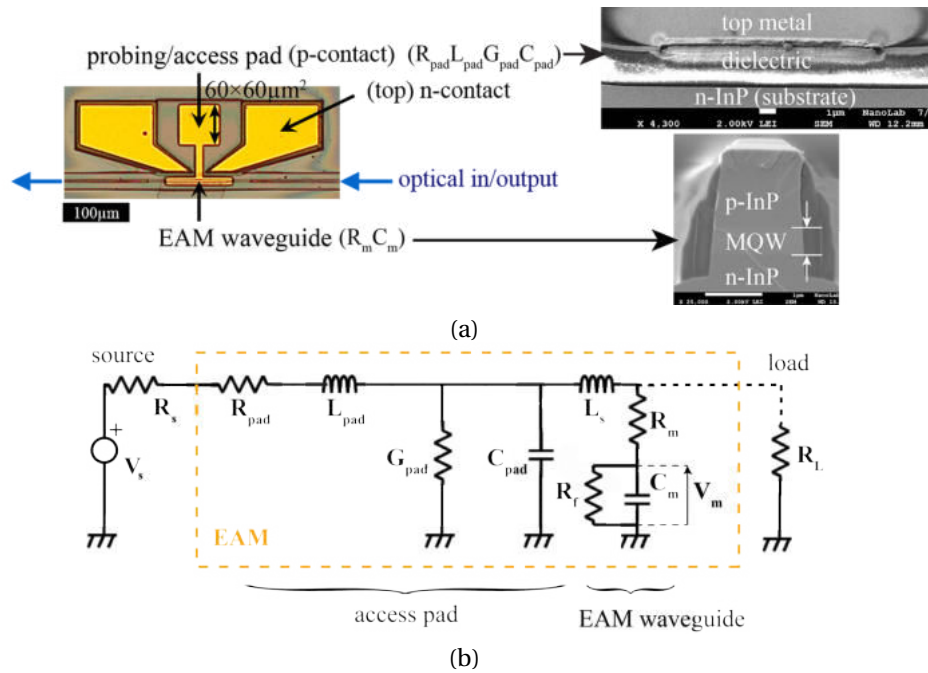


Figure 17.10: (a) Top-view of the fabricated electro-absorption modulator with probing/bonding pad next to it. (b) Equivalent electrical circuit model.

Two most common operations are usually regarded: semi-cooled and un-cooled operation of the modulator section. Semi-cooled operation usually requires operation in the range of temperatures $0-60^\circ\text{C}$, whereas un-cooled operation considers $0-100^\circ\text{C}$ [268, 269]. In this work, we test the modulator for semi-cooled operation.

17.4.3 Electrical design considerations

A fundamental requirement of an EAM in a transmission system is the ability to support the intended modulation format with a sufficient modulation bandwidth. The dynamic performance of an electro-absorption modulator is determined by its electrical frequency response and the available static extinction ratio. In the previous section on Mach-Zehnder modulators, a travelling wave configuration was considered. In here, we will consider the EAM as a lumped element model, as its length is much smaller than the operating RF wavelength ($L \ll \lambda_{RF}$).

17.4.3.1 Equivalent electrical circuit model

The active region of the modulator section is covered by the metal creating a p-type Ohmic contact for driving the EAM. The top metal is connected to the access pad, which serves as probing or wire-bonding pad, seen in Fig. 17.10a.

The frequency response of lumped electro-absorption modulator can accurately be predicted from an equivalent electrical circuit, shown in Fig. 17.10b [270]. EAM waveguide region consists of a series resistance R_m , junction capacitance C_m and photo-generated carriers R_f . The modulator series resistance includes the doped InP layers, and the junction capacitance describes the depletion region when an external reverse

bias is applied. The change of C_m with bias voltage needs to be taken into account, as it will result in different values. The photogenerated carriers have an effect on bandwidth when the input optical power level is high. In this case the carrier transit time increases due to a carrier pile-up and limits a high-speed operation. However, for low optical power levels we can neglect the effect of carrier transport and concentrate solely on the RC-limited response.

The access pad is represented as an RLGC-network element, where R_{pad} and G_{pad} represent the electric and dielectric loss, respectively. The modulator capacitance can be represented by a parallel plate capacitor:

$$C_m = \frac{\epsilon_0 \epsilon_r w L}{d} \quad (17.7)$$

where ϵ_r is the permittivity of intrinsic region, w waveguide width, L waveguide length and d intrinsic region thickness. A voltage generator is represented as an ideal source V_s with a series impedance R_s . R_L is a termination load placed at the output.

The extraction of the electro-absorption modulator equivalent electrical circuit can be done with a simple measurement of the reflection S_{11} parameter, described in [271]. The approach uses the analytical method to directly extract different circuit parameters over the whole measured frequency range.

17.4.3.2 3-dB bandwidth

A swept frequency RF signal is applied to the device through the bias T, combining DC and RF signals, to modulate the incoming continuous wave (CW) light. The modulated optical signal is detected by a fast photodiode and converted back in an electrical signal in the receiver part. The optical modulation and the reflected RF electrical signal are compared to the input RF electrical signal to determine the electro-optical (EO) transmission (S_{21}) and reflection (S_{11}) coefficient, i.e. the scattering (S) parameters of the device.

The device bandwidth is defined as the frequency range over which the magnitude of the S_{21} response remains within 3 dB with respect to the S_{21} value at $f = 0$. Considering the modulator resistance R_m is negligible compared to the generator R_g and load impedance R_L , it can be represented as a low-pass filter whose bandwidth is given by:

$$f_{3\text{dB}} = \frac{1}{2\pi \left(\frac{1}{R_g} + \frac{1}{R_L} \right)^{-1} (C_m + C_{\text{pad}})} \quad (17.8)$$

The junction and pad capacitance are dominant elements in the order of hundreds of fF. The junction capacitance scales with the device area, given by Eq. 17.7. The pad capacitance is determined by the layers underneath the metal.

The use of a termination resistor matched to the impedance of the source can minimize the reflection of RF power from the device [272]. Increasing R_L above the source impedance reduces the overall bandwidth, whereas its decrease improves the bandwidth but reduces the voltage across the junction and the RF power coupled to the device. The model is very helpful in understanding the basic limitations of the electro-absorption modulator design. Once the key parameters have been identified we can simply estimate the bandwidth of a given structure.

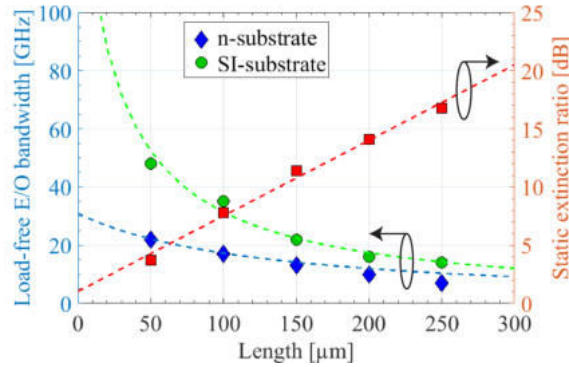


Figure 17.11: Trade off between the load-free EO bandwidth and static extinction ratio versus the modulator length.

17.4.4 Optical/electrical trade-off

A number of parameters influence the optical and electrical signal propagation in the electro-absorption modulator, described above. The most important optical parameter is the extinction ratio and the electrical is the bandwidth. However, a clear trade-off exists between the two parameters. Increasing the EAM length L improves the extinction ratio, but degrades the bandwidth. Fig. 17.11 shows measured values for the two parameters (symbols) depending on the modulator length and type of the substrate. The modulator intrinsic (load-free) bandwidth is considered.

The red dashed line is a linear fit of the static ER versus the EAM length. To achieve a static extinction ratio of 17 dB, the intrinsic bandwidth reduces to 8 GHz with 200- μm -long modulator. Shorter modulators of 50 μm provide 22 GHz, but only 4 dB static ER.

The green and blue dashed lines for load-free E/O bandwidth are calculated from the fitted values extracted from the S -parameter measurement. A clear advantage of semi-insulating substrate is seen at $L = 0$, representing the bandwidth of the access pad alone. On n-substrate the access pad limits the bandwidth to around 30 GHz, while on SI-substrate this value is as high as 160 GHz.

Electro-optical 3-dB bandwidth of the EAM itself without the access pad for lengths $L > 150 \mu\text{m}$ does not differ for n- or SI-substrate. It is because the modulator capacitance $C_m > 150 \text{ fF}$ becomes the dominant limiting factor. On the other side, at lengths $L < 150 \mu\text{m}$ the main difference between the substrates is created from the access pad behavior. Semi-insulating substrate shows doubled values of the available bandwidth.

To achieve both high extinction ratio and high bandwidth a larger number of quantum wells can be used. Increasing the quantum well number would benefit from the same design, having a bandwidth of 47 GHz, while having an increased static extinction ratio.

17.4.5 Electronic-Photonic matching

Driving a photonic integrated chip in a module can result in its different behavior than when tested on-chip. Module/package parasitics can limit the PIC performance by lowering the electro-optical bandwidth and increasing the reflection coefficient. For $>200\text{G}$ transmitters the operation in many cases involves (de)multiplexing of several 50 Gb/s electrical channels to/from a single $N \times 50 \text{ Gb/s}$ optical channel. Wavelength

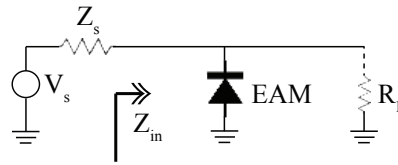


Figure 17.12: An EAM driven by a source V_s with internal impedance Z_s and an optional termination load R_L .

division multiplexing pushes the requirement of the electrical design side-by-side with the optical design. An efficient, low-reflection, routing of high-speed electrical signals from a centimeter scale connector to the micrometer level structures on the photonic integrated circuit (PIC) can present a design challenge.

In case of electro-absorption modulators (EAMs) a mismatch can exist between the EAM with a capacitive internal impedance, and a source with a real impedance. A typical source impedance is $50\ \Omega$, therefore the whole circuit seen from the source is desirable to have $50\ \Omega$ impedance to avoid the electrical signal back reflection. A typical implementation includes a parallel termination load of $50\ \Omega$ placed on- or off-chip. A monolithically integrated termination resistance can conveniently be utilized in integrated transmitters, reducing the footprint and package complexity [273]. However, an integrated termination load increases the power consumption on the PIC. Its placement outside of the chip after a capacitive element, decouples the power dissipation on-chip.

Making electrical connections between the electronic and photonic ICs can be performed in several ways, among which most common techniques are wire-bonding and stud-bump flip-chip bonding [274, 275]. Generally, wire-bonding is regarded to be a technologically easier process. However, parasitic effects due to the inductance of wire-bonds, may degrade the overall performance. The other commonly used option is a flip-chip technique, offering removal of wire-bond parasitics and a more compact integration on chip. Nevertheless, parasitic capacitances coming from the stud-bumps can limit the bandwidth [276].

The behavior of high speed electro-absorption modulators is highly dependent on the method of electrical interconnection, parasitic capacitance from the substrate and on wire-bond inductance or stud-bump capacitance. Once transferred to the PIC, high-speed signals must be routed from the bond pads to relevant components on the PIC. Hence, the design of on-chip transmission lines is of great relevance for high-speed operation and for densely integrated circuits as well. The perfect scenario is to simultaneously increase the EAM electro-optical bandwidth and minimize electrical reflections, by matching the input impedance seen from the source to its internal impedance.

17.4.5.1 Impedance matching

Impedance matching is a technique of optimizing the input impedance Z_{in} , seen from the source, in order to maximize the power transfer and minimize reflections back to the source. Fig. 17.12 illustrates the case of an electro-absorption modulator, with or without a termination load R_L .

The quality of an impedance match can be expressed mathematically by the reflection coefficient Γ_{in} :

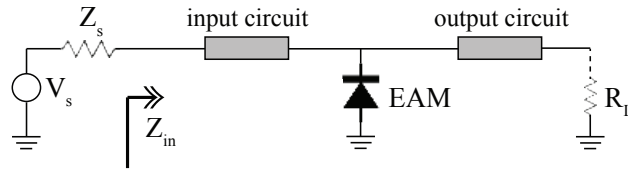


Figure 17.13: An added input and output circuit for the EAM internal frequency response improvement.

$$\Gamma_{in} = \frac{Z_{in} - Z_s}{Z_{in} + Z_s} \quad (17.9)$$

where Z_{in} is the modulator input impedance with or without termination load, and Z_s is the source impedance (very often, and in our case, equal to 50Ω). If the match is perfect ($Z_s = Z_{in}$), the numerator is zero, and the reflection coefficient is zero.

The power reflection coefficient can be expressed through $|\Gamma_{in}|^2$. Typical design values for the power input reflection coefficient are below -10 dB [253] for a good match between the driver and the chip in a wide frequency range.

The termination load, however, consumes DC power and increases the thermo-electric cooler power if placed on-chip. Decoupled termination can be achieved by placing it off-chip and inserting a capacitance for DC power decoupling. This configuration also allows to improve the electro-optic response. Since the modulator impedance is mainly capacitive, a circuit network can be inserted between the source and the EAM chip. The same thing can be done at its output, between the chip and the resistive load (Fig. 17.13). The goal is to achieve $Z_{in} = Z_s^*$. Matching networks can include a combination of transmission lines, termination load and other inductive/capacitive elements.

For more detailed information see [277].

17.4.5.2 Termination load placement

For assessing the EAM operation in an assembly or package the placement of the termination load can be used to improve the reflection coefficient. When the driver is integrated with the PIC, the termination load can be placed together with the driver, at the PIC input or at its output. Simulating the frequency response of the EAM in the generic platform, both cases are assessed: 1) R_L at the input connected via wire-bond L_{in} ; and 2) R_L at the output connected through a wire-bond L_{out} , and $L_{in} = 0$. For the first case, the wire-bond value is $L_{in} = 100$ pH corresponding to $\sim 100 \mu\text{m}$ wire-bond length (from experimental values), and for the second case $L_{out} = 300$ pH. Values are taken for an optimized frequency response of a $150\text{-}\mu\text{m}$ -long EAM, chosen as a compromise between high static extinction ratio and E/O bandwidth. Fig. 17.14 shows how the frequency response is influenced.

Simulating the termination load in front of the EAM shows an improvement of 4 GHz compared to the measurement with a 50Ω parallel load inside the RF probe. The termination load placed after the electro-absorption modulator results in an additional 6 GHz E/O bandwidth, and higher reflection coefficient bandwidth (below -10 dB) by 18 GHz. Therefore, its placement after the EAM is the preferred option for an improved frequency response.

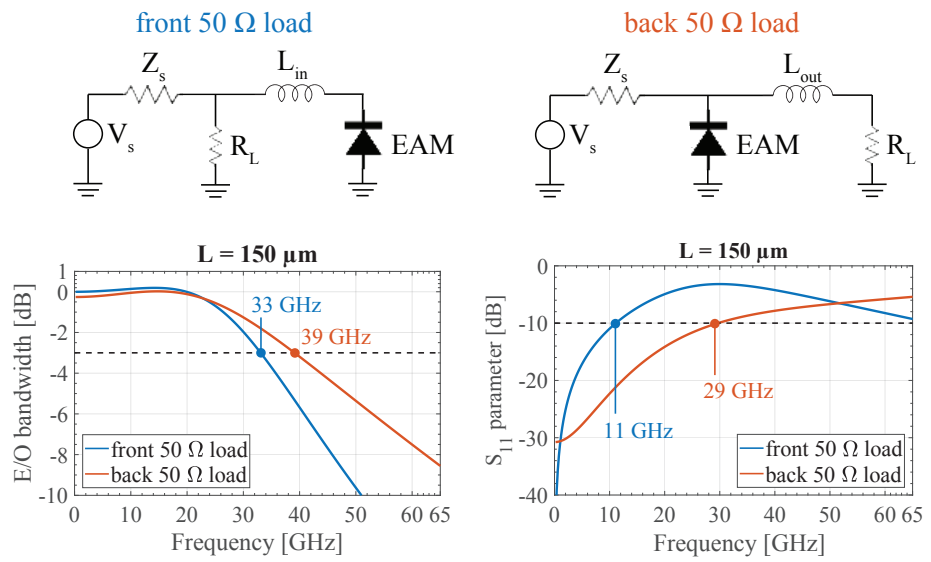


Figure 17.14: Termination load placed in front of the EAM and after it, and its simulated influence on the frequency response for a 150-μm-long EAM.